

Evolution of the Luminosity Function and Colours of Galaxies in a Λ Cold Dark Matter Universe

K. Nagamine,^{1*} † M. Fukugita,^{2,3} R. Cen,⁴ J. P. Ostriker,⁴

¹*Joseph Henry Laboratories, Physics Department, Princeton University, Princeton, NJ 08544, USA*

²*Institute for Cosmic Ray Research, University of Tokyo, Kashiwa 2778582, Japan*

³*Institute for Advanced study, Princeton, NJ 08540, USA*

⁴*Princeton University Observatory, Princeton, NJ 08544, USA*

5 September 2018

ABSTRACT

The luminosity function of galaxies is derived from a cosmological hydrodynamic simulation of a Λ cold dark matter (CDM) universe with the aid of a stellar population synthesis model. At $z = 0$, the resulting B band luminosity function has a flat faint end slope of $\alpha \approx -1.15$ with the characteristic luminosity and the normalization in a fair agreement with observations, while the dark matter halo mass function is steep with a slope of $\alpha \approx -2$. The colour distribution of galaxies also agrees well with local observations. We also discuss the evolution of the luminosity function, and the colour distribution of galaxies from $z = 0$ to 5. A large evolution of the characteristic mass in the stellar mass function due to number evolution is compensated by luminosity evolution; the characteristic luminosity increases only by 0.8 mag from $z = 0$ to 2, and then declines towards higher redshift, while the B band luminosity density continues to increase from $z = 0$ to 5 (but only slowly at $z > 3$).

Key words: galaxies: evolution – galaxies: formation – galaxies: fundamental parameters – galaxies: luminosity function, mass function – cosmology: theory

1 INTRODUCTION

The CDM model provides us with a basis of our understanding of cosmic structure formation and galaxy formation (Blumenthal et al. 1984; Davis et al. 1985). Much of the recent observational evidence points to a CDM universe dominated by a cosmological constant Λ (Efstathiou, Sutherland, & Maddox 1990; Ostriker & Steinhardt 1995; Turner and White 1997; Perlmutter et al. 1998; Riess et al. 1998; Balbi et al. 2000; Lange et al. 2001; Hu et al. 2001). The physics of galaxy formation, however, is substantially more complicated than the formation of large-scale structure for which an accurate treatment of gravity suffices. Many authors use the so-called semi-analytic models, in which the dark matter (DM) halo formation is supplemented with simple models of dissipative physics for baryons. Following the pioneering work of White & Frenk (1991), a series of the work (Baugh et al. 1998; Kauffmann et al. 1998; Somerville and Primack 1998; Cole et al. 2000) has shown that the model can account for many of the observed galaxy properties.

An alternative approach is to use cosmological hydrodynamic simulations directly. The advantage is that many physical processes are automatically taken into account with fewer model assumptions. The disadvantage, on the other hand, is that the method is computationally expensive, and the resolution is limited by computing power. However, the Eulerian hydrodynamic mesh is now approaching $(1000)^3$, and we are perhaps beginning to obtain meaningful results on the global properties of galaxies.

Adaptive Mesh Refinement (e.g., Bryan & Norman 1995; Kravtsov, Klypin, & Khokhlov 1997) and Smoothed Particle Hydrodynamics (e.g., Katz, Weinberg, & Hernquist 1996) have virtues intermediate between the two listed approaches. They solve the hydrodynamic equations directly and have a spatial resolution better than the Eulerian scheme, but they have a mass resolution coarser than the Eulerian scheme adopted in this paper. Semianalytic models which are based on dark matter halo merger trees in N -body simulations also suffer from mass resolution limits.

In a preceding publication (Nagamine, Fukugita, Cen, & Ostriker 2001, hereafter Paper I), we discussed galaxy formation history, with a special emphasis given to the star formation history and the stellar metallicity distribution. In this article, we focus our attention to the luminosity function (LF) and its evolution, which allows comparison with

* Present address: Harvard College Observatory, 60 Garden Street, MS 51, Cambridge, MA 02138, U.S.A.

† Email: nagamine@astro.princeton.edu

one of the most fundamental aspects of galaxy observations. We supplement our cosmological simulation with a population synthesis model GISSEL99 (Bruzual & Charlot 1993, ; Charlot 1999, private communication), which takes metallicity variations into account. We assume that stars form from gas as soon as the cooling conditions are satisfied. The Salpeter (1955) initial mass function (IMF) with a turnover at low-mass end reported by Gould, Bahcall, & Flynn (1996, hereafter GBF) is assumed. The results are presented in the standard Johnson-Morgan photometric system.

2 SIMULATION AND PARAMETERS

The hydrodynamic cosmological simulation we use in this paper is the same as that used in Paper I; the comoving box size is $25h^{-1}$ Mpc, with 768^3 grid cells and 384^3 dark matter particles each of mass $2.03 \times 10^7 h^{-1} M_\odot$. The comoving cell size is $32.6h^{-1}$ kpc, and the mean baryonic mass per cell is $3.35 \times 10^5 h^{-1} M_\odot$. The cosmological parameters are chosen to be $(\Omega_m, \Omega_\Lambda, \Omega_b h^2, h, \sigma_8) = (0.3, 0.7, 0.016, 0.67, 0.9)$. The basic structure of the code is similar to that of Cen & Ostriker (1992a,b), but significantly improved over the years (see Cen & Ostriker 2000).

We also use a simulation with 384^3 grid cells (factor 2 and 8 lower spatial and mass resolution, respectively) to assess the effect of the resolution on our result. We call the higher resolution run as ‘‘N768’’, and the other ‘‘N384’’. The input parameters are kept to be same for the two runs except the resolution.

The details of the star formation recipe, the energy feedback, and the metal production treatments are described in Paper I, so we do not repeat them here. The adopted yield $Y = 0.02$ (Arnett 1996) dominantly controls the resulting amount of stars ($\Omega_* = 0.0052$ including the 25% ejected gas by supernovae) and the metal density, which are consistent with the upper limit of the empirical estimate of Fukugita, Hogan, & Peebles (1998). We identify galaxies and DM halos using the HOP grouping algorithm (Eisenstein & Hut 1998) with the same threshold parameters as in Paper I. We refer to the grouped stellar particles as ‘galaxies’ hereafter. We confirmed that all galaxies identified by HOP are dynamically stable enough to obtain meaningful results for the evolution of individual galaxies (see Paper I).

3 MASS AND LUMINOSITY FUNCTION AT $Z = 0$

In Figure 1, we show the DM halo mass function $\Phi(M)$ in dash-dotted (N768) and short-dashed (N384) histograms. The galaxy stellar mass function $\Phi_g(M)$ is also shown in solid (N768) and dotted (N384) histograms at $z = 0$, where $\Phi(M)d\log(M) \equiv \phi(M)dM$ (likewise for the LF below). The two long-dashed lines show $\phi(M) \sim M^{-2}$ and $\phi_g(M) \sim M^{-1.15}$.

The DM halo distribution follows $\phi(M) \sim M^{-2}$ well, which is the generic mass distribution of the hierarchical clustering model. Some rounding at the low mass end is seen below $10^{10} M_\odot$ (500 DM particles), and a slight overproduction of massive halos is seen at above $10^{13} M_\odot$ due to overmerging problem.

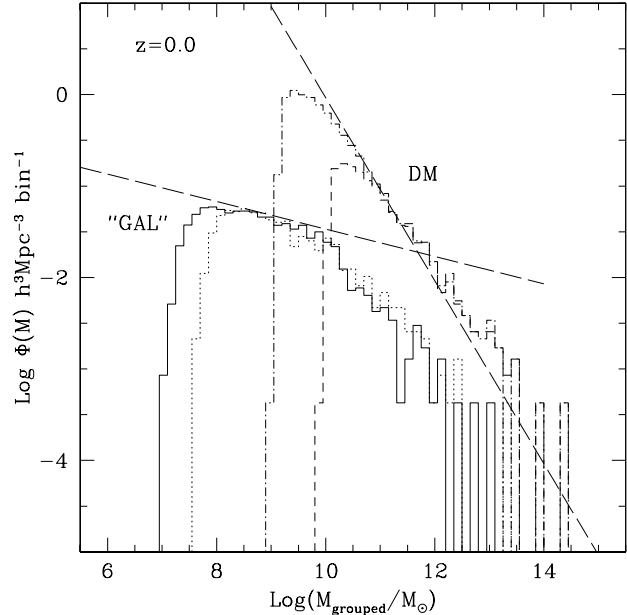


Figure 1. Mass function of dark matter halos (dash-dotted N768 & short-dashed N384 histogram) and galaxy stellar mass (solid N768 & dotted N384 histogram). The two long-dashed lines show $\phi(M) \sim M^{-2}$ and $\phi_g(M) \sim M^{-1.15}$.

The galaxy stellar mass function behaves quite differently: flattening below $10^{10} M_\odot$ is apparent, which can be ascribed to supernova feedback (Dekel & Silk 1986) and photoheating of gas (Rees 1986; Efstathiou 1992), both more efficient in less massive galaxies. The results of N768 and N384 agree well in the overlapping mass range for both the dark matter and the galaxy stellar mass functions, verifying that the results that concern us in this paper are not strongly affected by the resolution effects. Therefore, only N768 run is used in the rest of this paper.

At above $3 \times 10^{10} M_\odot$, the galaxy stellar mass function departs from the power law and seems to follow DM halo mass function. This departure from the faint-end power law can partly be ascribed to the inefficient cooling in massive galaxies (Rees & Ostriker 1977; Silk 1977). The cutoff at high-mass end, however, is not quite exponential; there are several objects with a very large stellar mass of $> 5 \times 10^{11} h^{-1} M_\odot$ (indicated by the dotted histogram), due to an overmerging problem. These objects have the mass of groups and clusters, and the galaxies have overmerged in very high-density regions due to the limited spatial resolution of the simulation. There is no good way to decompose the overmerged objects into individual galaxies, and it is difficult to estimate the effect of the overmerging to the shape of the high-mass end of the stellar mass function.

The LF in the rest-frame B band (before dust extinction) is presented in Figure 2 as a function of absolute magnitude (the overmerged objects with stellar mass $> 5 \times 10^{11} h^{-1} M_\odot$ are indicated by the dotted histograms). We attempt to fit the Schechter function to the computed LF in the following manner: the faint end slope α is fixed to -1.15 throughout this paper, we then choose ϕ^* to fit the faint end plateau of the LF, and adjust M_B^* so that the chosen Schechter function reproduces the computed luminosity density when it is integrated over. Al-

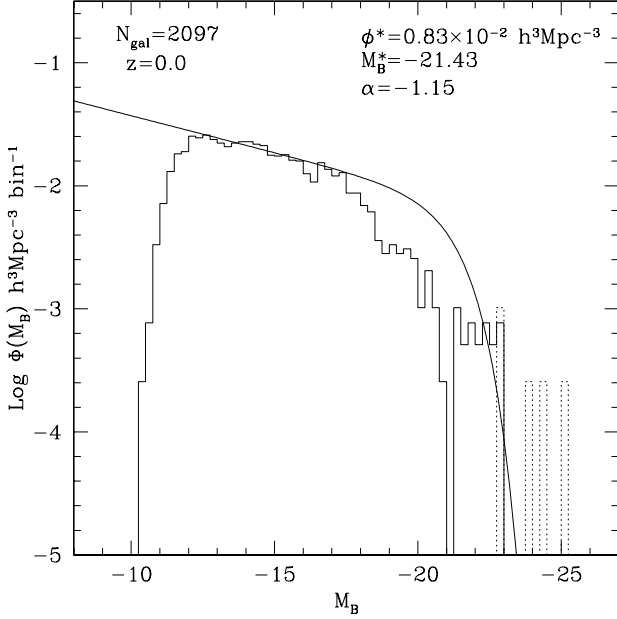


Figure 2. Luminosity function of galaxies at $z = 0$. The galaxies with stellar mass of $> 5 \times 10^{11} h^{-1} M_{\odot}$ are shown as dotted histogram, and the solid curve is the Schechter function with the indicated parameters in the figure. See text for the method of the fitting.

though the overmerging problem hampers accurate determination of the Schechter parameters of the computed LF, they can still be used to characterize our result with a minimum number of adjustable parameters. In the figure, the Schechter function with $\alpha = -1.15$, $M_B^* = -21.43$, and $\phi^* = 0.83 \times 10^{-2} h^3 \text{Mpc}^{-3}$ is shown in the solid curve. The simulated LF fits the slope of $\alpha = -1.15$ well at fainter magnitudes below $M_B = -17$. If the overluminous objects are not included in the fit, then we obtain $M_B^* = -20.68$, which is 0.75 magnitude dimmer than the case of full luminosity. This may suggest that our M_B^* at $z < 1$ is biased towards the brighter side because of the overmerged objects.

The computed B band luminosity density \mathcal{L}_B of galaxies at $z = 0$ is $2.4 \times 10^8 h L_{\odot,B} \text{Mpc}^{-3}$ including the overmerged objects. A source of large uncertainty in the luminosity density is the assumed IMF. The use of Salzo IMF instead of the Salpeter IMF would increase the computed \mathcal{L}_B by $\sim 30\%$ (White & Frenk 1991). Another source of uncertainty is the dust extinction. The empirical average value of extinction in the B band is $A_B = 0.33$ mag (de Vaucouleurs, et al. 1991). The corresponding decrease in \mathcal{L}_B by dust extinction is by 30%.

Optical surveys of galaxies have made significant progress over the last 10 years. In particular, the 2dF Survey (Cross et al. 2000) and the Sloan Digital Sky Survey (Blanton et al. 2001; Yasuda et al. 2001) have secured the luminosity functions and the local luminosity density of the universe. Both surveys agree on $\alpha = -1.20 \pm 0.10$ and $M_B^* = -19.8 \pm 0.2 + 5 \log h$, and the luminosity density $\mathcal{L}_B = 2.4 \pm 0.4 \times 10^8 h L_{\odot,B}$. Our M_B^* at $z = 0$ is brighter than empirical values by 0.76 magnitude, and ϕ^* is lower by a factor of ~ 2 . Overmerged objects contribute about 50% of the total luminosity in the box, but the overmerging does not affect the total luminosity density, as the fraction

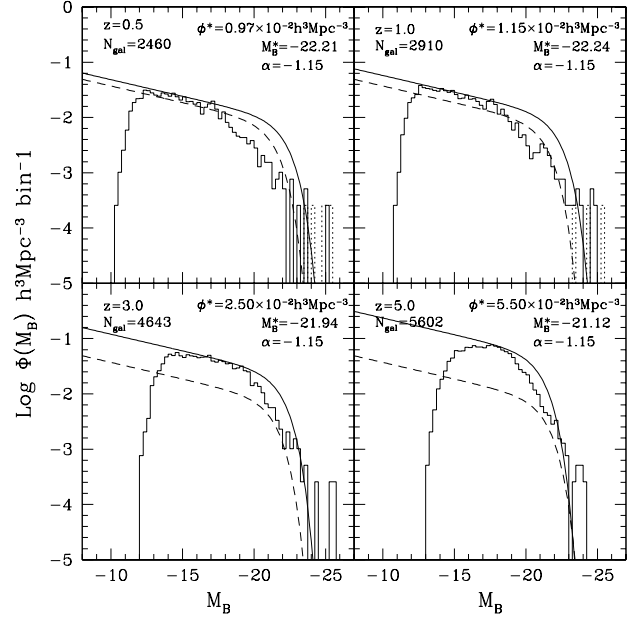


Figure 3. Luminosity function of galaxies at $z = 0.5, 1, 3$, and 5 . The ‘galaxies’ with stellar mass $> 5 \times 10^{11} h^{-1} M_{\odot}$ are shown as dotted histograms. The solid curves are the Schechter functions with the indicated parameters in each panel, and the dashed curve is the Schechter fit to the simulated LF at $z = 0$ shown in Figure 2.

of baryons that condense into stars is basically determined by the yield parameter in the simulation (see Paper I).

The uncertainty in the fitted value of M_B^* associated with the overmerging, IMF, and dust extinction is of the same order as the above discrepancy between the computed and the observed LF. In view of the fact that we have not fine-tuned the simulation parameters, we consider the agreement of the computed LF and \mathcal{L}_B with observations is fair.

4 EVOLUTION OF LUMINOSITY FUNCTION

Figure 3 shows the rest-frame B band LF at $z = 0.5, 1, 3$, and 5 . The solid curves are the Schechter functions with the indicated parameters (see also Table 1), chosen in the same manner as in Figure 2. The dashed curve is the Schechter function at $z = 0$ for comparison.

We observe some evolution between $z = 0$ and 1 . The characteristic magnitude M_B^* brightens by 0.8 mag, and the normalization ϕ^* increases by a factor of 1.4. As a result, \mathcal{L}_B at $z = 1$ is 2.9 times higher than at $z = 0$ (Table 1). The faint end slope evolves very little.

We find that the evolution of the LF is different from that of the galaxy stellar mass function, which is also fitted well by the Schechter function except at the high-mass end. The characteristic mass M_g^* of the galaxy stellar mass function decreases by a factor of 2.4 from $z = 0$ to 1 , but the number of galaxies increases by a factor of 1.4, leading to a moderate decrease in the stellar mass density ρ_* by a factor of 1.5 (Table 1). These changes are compensated by the luminosity evolution: the average B band mass-to-light ratio of galaxies decreases by a factor of 2.4, leading to more luminous L_B^* at higher redshift. The increase of luminosity to higher redshift is due to increased star formation of blue

galaxies (Paper I), but it is also partly due to the passive evolution of red galaxies, as evidenced from the shift of the red edge in the colour distribution, as we see below.

Empirical knowledge of the evolution of the LF is still controversial, despite much effort made by the Canada-France Redshift Survey (CFRS; Lilly et al. 1995), the Autofib Redshift Survey (Ellis et al. 1996), the CNOC2 Survey (Lin et al. 1999), the CADIS Survey (Fried et al. 2001), and the DEEP project (Davis, et al. 2000). The CFRS and the CADIS claim that the blue population brightens by about 1 magnitude from $z = 0$ to 0.8, while the characteristic luminosity changes little for the red population. On the other hand, the CNOC2 and the DEEP claim brightening of characteristic luminosity for red (or early) populations. The Autofib indicates little evolution of L_B^* for total luminosity function, while it claims steepening of the faint end slope.

Overall, we summarize that the change in L_B^* from $z = 0$ to 1 deduced from the observations for the total LF is modest, no more than ~ 1 mag in the Λ cosmology, whereas the appreciable increase in luminosity density is common to all surveys. The values of luminosity density are discrepant among authors, and their low-redshift values are also not consistent with what we referred to for $z = 0$ above. By compiling all results, we conclude that the increase of \mathcal{L}_B from $z = 0$ to 0.5 is by a factor of 1.4 – 2, and by a factor of 2 – 3 from $z = 0$ to 1. The result from our simulation is consistent with these data at the upper end for both L_B^* and \mathcal{L}_B . We have not seen steepening of the total LF towards higher redshift in our simulation.

The trend of evolution is somewhat different when one goes to higher redshift. The characteristic mass of the galaxy stellar mass function decreases more rapidly from $z = 1$ to 3 (by a factor of 6). This change is faster than that of the mass-to-light ratio, resulting in a moderate decrease of the characteristic luminosity. The normalization of the LF increases rapidly towards higher redshift, but the increase in \mathcal{L}_B is smaller above $z = 2$, because galaxies become less massive and dimmer at the same time.

We find that the U -band luminosity density continues to increase from $z = 0$ to 5, whereas the K -band luminosity density gradually decreases towards high-redshift, at least from $z = 2$ (some increase is observed from $z = 0$ to 1).

5 GALAXY COLOURS AND THEIR EVOLUTION

Figure 4 presents the $B - V$ colour distribution of galaxies at various redshifts. At $z = 0$, the $B - V$ colour ranges from 0.55 to 0.95 with a tiny fraction of galaxies (0.6% in number, but 12% in luminosity) bluer than 0.5 that represents very active star-forming galaxies. The median $B - V$ is 0.70. These results are in global agreement with observations for local galaxies, which ranges from $B - V = 0.45$ (the bluest Im) to 1 (giant E); $B - V = 0.7$ is the median colour of Sb galaxies (Buta et al. 1994; Fukugita, Shimasaku, & Ichikawa 1995). In finer details, the calculated distribution is slightly narrower than the observations in both blue and red edges.

As one goes to higher redshift, the red edge is shifted, which is ascribed to the younger age of galaxies, since the red edge is mainly determined by the maximal available time for passive evolution of galaxies up to each epoch. The shape of

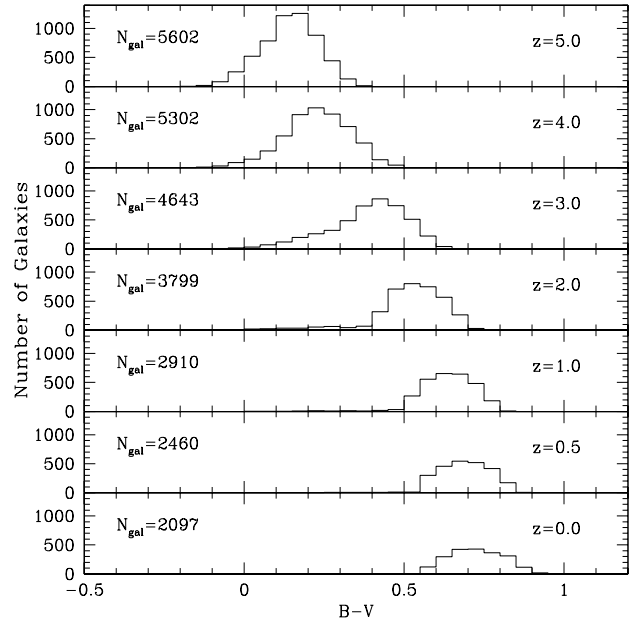


Figure 4. Rest-frame $B - V$ colour distribution of galaxies at various redshifts. See text for discussions.

the distribution on the red side does not change very much as a function of redshift. Another conspicuous fact as one goes to higher redshift is the increasingly longer tail towards the blue side, indicating star formation in larger fractions of galaxies. At high-redshift, this star-forming population rapidly increases, and at $z = 4$ the bulk of the population is star-forming. In addition to the increasing star formation, the stellar population tends to be bluer due to lower metallicity at high-redshift (see Paper I).

The $U - B$ colour at $z = 0$ ranges from -0.05 to 0.4 in good agreement with local observations, except that it is a little narrower than the observations (Buta et al. 1994; Fukugita et al. 1995). The evolution is qualitatively similar to $B - V$. Assuming a typical extinction parameter of $R_V = 3.1$ and the extinction law of Cardelli, Clayton, & Mathis (1989), one finds that the $U - B$ colour becomes redder by 0.06 mag.

The $V - K$ colour at $z = 0$ ranges from 1.9 to 2.9. This is perhaps bluer by 0.1 mag at the red edge, and 0.3 mag bluer at the blue edge than the real world (Fioc & Rocca-Volmerange 1999). This bluer colour is ascribed to the GISSEL99 model, with which $V - K$ colour 1 Gyr after the burst is only 2.0, and that at 14 Gyrs is 3.0 for a galaxy with 40% solar metallicity (see Paper I for the metallicity of galaxies in our simulation).

6 DISCUSSION

Our Λ CDM simulation reproduces the global statistics concerning the luminosity and colours of galaxies fairly well at $z = 0$ considering the uncertainties in the model and the simulation. Even the current level of agreement is a significant improvement over the previous simulations, and we are satisfied with the qualitative agreement for the moment, given that we have not done the fine-tuning of the input parameters.

Table 1. GALAXY STATISTICS PARAMETERS

Quantities	$z = 0$	$z = 0.3$	$z = 0.5$	$z = 1$	$z = 2$	$z = 3$	$z = 5$
M_B^*	-21.43	-21.93	-22.21	-22.24	-22.27	-21.94	-21.12
ϕ^*	0.83	0.93	0.97	1.15	1.60	2.50	5.50
\mathcal{L}_B	1.62	2.86	3.86	4.69	6.74	7.77	8.02
$\langle M/L_B \rangle$	4.3	3.2	2.7	1.8	0.87	0.44	0.16
$\langle M/L_K \rangle$	1.3	1.0	0.91	0.69	0.42	0.30	0.21
ρ_*/\mathcal{L}_B	4.0	2.1	1.4	0.94	0.44	0.25	0.13
ρ_*/\mathcal{L}_K	0.77	0.53	0.49	0.39	0.27	0.21	0.15
$\langle B - V \rangle$	0.70	0.68	0.66	0.61	0.50	0.36	0.12
$\langle U - B \rangle$	0.09	0.07	0.06	0.05	0.03	-0.03	-0.28
$\langle V - K \rangle$	2.29	2.23	2.18	2.09	1.92	1.68	1.20
M_g^*	2.34	1.97	1.45	0.97	0.41	0.16	0.05
ϕ_g^*	0.83	0.93	1.10	1.35	2.20	3.60	6.00
ρ_g^*	6.50	6.13	5.34	4.39	3.00	1.98	1.03

Parameters of the Schechter functions shown in Figure 2 and 3 are presented in the first two rows. α is fixed to -1.15 in all cases. See text for the method of choosing the values of M_B^* [mag] and $\phi^*[10^{-2}h^3 \text{Mpc}^{-3}]$. \mathcal{L}_B is in units of $[10^8 L_{\odot,B} \text{Mpc}^{-3}]$ with $h = 0.67$. The average mass-to-light ratio of all galaxies in solar units, and the average of the entire box (mass density divided by luminosity density) are also given. The Schechter parameters of the galaxy stellar mass function ($M_g^*[10^{11} M_{\odot}]$ and $\phi_g^*[10^{-2}h^3 \text{Mpc}^{-3}]$) and the comoving stellar mass density $\rho_g^*[10^8 M_{\odot} \text{Mpc}^{-3}]$ are shown in the bottom three rows.

The number evolution and the luminosity evolution of galaxies takes place at the same time in the simulation. The galaxies in the simulation continues to become less massive and more numerous from $z = 0$ to 5, as expected in the hierarchical structure formation scenario, but luminosity per stellar mass significantly increases to high redshifts. Because of the compensation of the two effects, the change in the LF is modest: the characteristic luminosity increases from $z = 0$ to 2 only by 0.8 mag, and then decreases beyond $z > 2$. The evolution of the LF is a modest representation of the evolution of individual galaxies. The B band luminosity density continues to increase from $z = 0$ to 5, but only slowly at $z > 3$. We do not see the apparent steepening of the faint end slope of the LF. Uncertainties in the observational LFs at non-zero redshifts do not allow a finer comparison of the model prediction with the data.

In detailed level the agreement between the predictions and the observations is not perfect. However, given the uncertainties in the theoretical modelling and observations, the level of agreement presented in this paper is encouraging. The qualitative evolutionary trends presented in this paper (and those in Paper I) can be taken as predictions of hydrodynamic simulations based on the Λ CDM model plus the prescriptions for star formation and feedback effects. These qualitative predictions can be used to test the Λ CDM scenario against further observational studies.

ACKNOWLEDGMENTS

We thank Michael Strauss for useful comments on the draft. K.N. is supported in part by the Physics Department. M.F. is supported in part by the Raymond and Beverly Sackler Fellowship in Princeton and Grant-in-Aid of the Ministry of Education of Japan. R.C. and J.P.O. are partially supported by grants AST 98-03137 and ASC 97-40300.

REFERENCES

- Arnett D., 1996, *Supernovae and Nucleosynthesis*, Princeton University Press, pp.496
- Balbi A., et al., 2000, ApJ, 545, L1
- Baugh C. M., Cole S., Frenk C. S., Lacey C. G., 1998 ApJ, 498, 504
- Blanton M. R., et al., 2001, AJ, 121, 2358
- Blumenthal G. R., Faber S. M., Primack J. R., & Rees M. J., 1984, Nat, 311, 517
- Bruzual A. G., Charlot S., 1993, ApJ, 405, 538
- Bryan G. L., Norman, M. L., 1995, AAS, 187.9504
- Buta R., Mitra S., de-Vaucouleurs G., Corwin JR. H. G., 1994, AJ, 107, 118
- Cardelli J. A., Clayton G. C., Mathis J. S., 1989, ApJ, 345, 245
- Cen R., Ostriker J. P., 2000, ApJ, 538, 83
- Cen R., Ostriker J. P., 1992a, ApJ, 393, 22
- Cen R., Ostriker J. P., 1992b, ApJ, 399, L113
- Cole S., Lacey C., Baugh C., Frenk C., 2000, MNRAS, 319, 168
- Cross N., et al., 2000, MNRAS, 324, 825
- Davis M., Newman J., Faber S., Phillips A., 2000, Proc. of the ESO/ECF/STSCI workshop on Deep Fields (Springer), in press (astro-ph/0012189)
- de Vaucouleurs G., et al., 1991, *Third Reference Catalogue of Bright Galaxies*, Springer-Verlag, p.31
- Efstathiou G., 1992, MNRAS, 256, L43
- Davis M., Efstathiou G., Frenk C. S., White S. D. M., 1985, ApJ, 292, 371
- Dekel A., Silk, J., 1986, ApJ, 303, 39
- Efstathiou G., Sutherland W. J., Maddox S. J., 1990, Nat, 348, 705
- Eisenstein D. J., Hut P., 1998, ApJ, 498, 137
- Ellis R. S., Colless M., Broadhurst T., Heyl J., Glazebrook K., 1996, MNRAS, 280, 235
- Fioc M., Rocca-Volmerange B., 1999, A&A, 351, 869
- Fried J. W., et al., 2001, A&A, 367, 788
- Fukugita M., Hogan C. J., Peebles P. J. E., 1999, ApJ, 503, 518

- Fukugita M., Shimasaku K., Ichikawa T., 1995, *PASP*, 107, 945
- Gould A., Bahcall J. N., Flynn C., 1996, *ApJ*, 465, 759
- Hu W., Fukugita M., Zaldarriaga M., Tegmark M., 2001, *ApJ*, 549, 669
- Kauffmann G., Colberg J. M., Diaferio A., White S. D. M., 1999, *MNRAS*, 303, 188
- Katz N., Weinberg D. H., Hernquist L., 1996, *ApJ*, 105, 19
- Kravtsov A. V., Klypin A. A., Khokhlov A. M., 1997, *ApJ*, 111, 73
- Lange A. E., et al., 2000, *Phys.Rev. D*63, in press (astro-ph/0005004)
- Lilly S. J., Tresse L., Hammer F., Crampton D., Le Fevre O., 1995, *ApJ*, 455, 108
- Lin H., et al., 1999, *ApJ*, 518, 533
- Nagamine K., Fukugita M., Cen R., Ostiker J. P., 2001, *ApJ*, in press (astro-ph/0011472; Paper I)
- Ostriker J. P., Steinhardt P. J., 1995, *Nat*, 377, 600
- Perlmutter S., et al., 1998, *Nat*, 391, 51
- Riess A. G., et al., 1998, *AJ*, 116, 1009
- Rees M. J., 1986, *MNRAS*, 218, 25
- Rees M. J., Ostriker J. P., 1977, *MNRAS*, 179, 541
- Salpeter E. E., 1955, *ApJ*, 121, 161
- Rieke G. H., Lebofsky M. J., *ApJ*, 288, 618
- Silk J., 1977, *ApJ*, 211, 638
- Snedden C., Gehrz R. D., Hackwell J. A., York D. G., Snow T. P. 1978, *ApJ*, 223, 168
- Somerville R. S., Primack J. R., 1999, *MNRAS*, 310, 1087
- Steidel C. C., Adelberger K. L., Giavalisco M., Dickinson M., Pettini M., 1999, *ApJ*, 519, 1
- Steidel C. C., Adelberger K. L., Dickinson M., Giavalisco M., Pettini M., Kellogg M., 1998, *ApJ*, 492, 428
- Turner M. S., White M. 1997, *Phys. Rev. D*, 56, 4439
- White S. D. M., Frenk C. S., 1991, *ApJ*, 379, 52
- Yasuda N., et al., 2001, *AJ*, submitted (astro-ph/0105545)

This paper has been typeset from a \LaTeX file prepared by the author.